Magnesium AZ31 alloy coating for bone implant applications

Authors: Francisco Albuquerque
Instituto Superior Técnico/CQE/DEQ
Lisboa, Portugal
fpsalbuquerque@gmail.com

Abstract: ***Thanks to its biocompatibility and mechanical properties close to cortical bone, magnesium alloys are a promising candidate to bone implants materials. However, due to its fast corrosion rates, nowadays it still not possible for magnesium to withstand all the structural requirements of bone healing for enough time. This work consists in tailoring the magnesium alloy surface through a plasma electrolytic oxidation (PEO) followed by a hydrothermal treatment, thus increasing its corrosion resistance. SEM-EDS and XRD techniques were used to characterize the surface morphology, chemical composition and phase distribution. EIS in 0.1M NaCl solution and SBF were performed to evaluate the corrosion behaviour and apatite forming ability.***

Key words: *Magnesium, Biodegradable implants, Hydroxyapatite, Electrochemical impedance spectroscopy, Plasma electrolytic oxidation, hydrothermal treatment, Simulated body fluids*

INTRODUCTION

Biomaterials can be defined as men made or natural origin materials that scope to substitute or repair human body parts, and one of the most challenging application for implant materials is bone repairing [1]. There are two main groups of biomaterials, which are the bio-inert ones and the bio-degradable ones. The first group is used nowadays with high success rates, however they carry the problem that, due to the very long periods that those stay inside the human body, they often need a second surgery to remove the implant [2]. The second group do not carry this problem, however, since the golden standard for those materials is the transplant of bone tissue, it has the disadvantages of being a more complicated surgery, having a limited bone supply, and donor site morbidity (when the material used is transplanted from one body part to another) or bacterial infections, non-union due to different bone qualities (when the material comes from a cadaver) [3, 4].

Due the natural bone transplanting drawbacks, there is a major effort to improve synthetic scaffolds for bone grown. Those are divided in polymers, like PLA or natural collagen, which exhibit very good biocompatibility, however they lack mechanical properties required for the structural functions of bone, and tend to degrade to rapid; Ceramic materials, like bio glasses, can maintain their properties during the bone healing period, but their low fracture toughness is a major drawback; and metallic material, like titanium alloys, that can withstand all the mechanical requirements, however several issues can arise from the young modulus mismatch like bone shielding, and the constant release of corrosion products and gases evolution, into the surrounding tissues can be to large for the body to deal with [3, 5].

The use of composite biomaterials can combine several advantages like good biocompatibility of calcium phosphates with the high fracture toughness of metals.

Magnesium and its alloys have a high potential of being used for bone implants, since their mechanical properties are relatively close to cortical bone and their corrosion products have been proven to be biocompatible and easily removed by the urinary system. However, their extremely high corrosion rates leads to a fast loss of their mechanical properties and the gaseous hydrogen release into the surrounding tissues may be to large for the body to deal [4].

The scope of this work is to tailor and characterise the surface of magnesium AZ31 alloy trough plasma electrolytic oxidation (PEO) followed by a hydrothermal treatment (Ht), improving its properties as a biodegradable orthopaedic material.

I. EXPERIMENTAL

A. Plasma electrolytic oxidation (PEO)

The samples used in this treatment were cut from a wrought magnesium AZ31 rod and then a copper wire was glued on one side with high purity silver paint of SPI®. After that the samples were imbedded in epoxy resin to isolate the alloy/wire junction. This alloy was chosen due to its low content in toxic elements, such as aluminium, and superior mechanical properties when compared to other Mg alloys. The nominal composition in wt% of this alloy is: Al 2.5 – 3.5; Zn 0.5 – 1.5; Si 0,1; Fe 0.03; Ni 0.05; Mn 0.05 – 0.4; others 0.1; Mg balance.

Before the treatment all samples were polished with SiC emery paper of 400, 800, 1000 and 2500, cleaned with alcohol and dried in air.

The PEO treatments were performed with an Agilent® 6813B AC power source, with the maximum power of 1750 VA. The cell consisted in a laboratory glass beaker of 1L and the solution temperature was kept at 10 ± 0.5ºC by using a Julabo® refrigerator that kept a cooling oil flowing through a 316 stainless-steel tubular spring. The specimens were connected to the positive pole, as an anode, and the cathode was the SS 316 spring. All the solution compositions and electrical parameters are listed in table 1, and the duty cycle of all anodizations was 20%. The exposed areas that were covered had an area of 2.25cm^2.

Table 1 – Electrical and electrolyte parameters for the PEO treatment.

		Sample Designation							
		1A	**1B**	**2A**	**2B**	**3A**	**3B**	**4A**	**4B**
Solution (g/L)	**Na_3PO_4**	10	10	20	20	10	10	20	20
	KOH	2	2	4	4	-	-	-	-
	$Ca(OH)_2$	-	-	-	-	2	2	2	2
	I (A/cm²)	0.08	0.25	0.08	0.25	0.08	0.25	0.08	0.25
	V_{max} (V)	340	421	292	382	354	421	299	411

B. Hydrothermal treatment

The two samples that showed a higher corrosion resistance were subjected to two hydrothermal treatments that were performed in an aqueous solution containing 0.1M of Ca-EDTA and 0.1M of KH_2PO_4. The pH was adjusted to 9.5, Ht_1 and 8.5, Ht_2, with a 1M NaOH solution.

C. Thickness measurement

The thickness was measured in every sample before and after the Hts and the immersion tests. The equipment used was a thickness coating gauge from Elcometer®.

D. Morphology and chemical composition characterization

All samples were evaluated with a Hitachi® S2400 analytical SEM, equipped with a Bruker® light elements EDS detector. Also, before and after the Hts and the immersion tests.

Phase analysis was performed using a Philips PW diffractometer, the radiation used was CuKα, with a wave length of 1.5842Å, with a power of 30W and 40mA, an increment of 0.01º, with a rate of one step per second. The measurement took place in the range of 10º - 20º in a continuous mode. All the diffraction patterns obtained were compared with patterns present both in the software Match® and the free online database RRUFF.

E. Electrochemical tests

The corrosion behavior was assessed by electrochemical impedance spectroscopy (EIS), with a Gamry® Reference 600 Plus, and the software was Gamry Framework, at open circuit potential, versus a calomel reference electrode and a platinum counter electrode. The starting frequency was 10^5Hz and the final was 0.01, with 9 points per decade.

The first round of EIS was measured with a 0.1M NaCl solution after an immersion of 24h at 24ºC inside a faraday cage.

The second round was performed in simulated body fluids (SBF) at 37ºC inside a Memmert® HPP260 oven. Open circuit potential (OCP) of the first 12h and one hour before the end of each day was measured followed by an EIS measurement.

All the impedance data was analysed with the software Zview.

II. Results and Discussion

A. Thickness measurement

Table 2 list the average thicknesses obtained after each PEO treatment and table 3 lists the average thickness after Ht, and and after SBF immersion.

Table 2 - Average thicknesses obtained for all the PEO coatings.

Sample	**1A**	**1B**	**2A**	**2B**	**3A**	**3B**	**4A**	**4B**
Thickness (µm)	14.53	28.37	19.37	49.22	12.50	22.62	20.20	43.23

Table 3 - Average thicknesses obtained for Ht and SBF immersion samples.

Sample	**2B SBF**	**4B SBF**	**2BHt1**	**2BHt1 SBF**	**2BHt2**	**2BHt2 SBF**	**4BHt1**	**4BHt1 SBF**	**4BHt2**	**4BHt2 SBF**
Thickness (µm)	45.33	48.53	51.57	52.07	51.33	53.23	47.9	49.37	47.5	51.83

As expected from literature, the thickness of the PEO coatings increased both with the solution composition and the current intensity. After the hydrothermal treatments, sample 2B didn't present a substantial increase in thickness, on both treatments, increasing approximately 2µm, and the sample 4B thickness increase was about 4µm, also on both treatments. Those results suggest that one value of pH on the hydrothermal treatments has no influence on the coatings thickness. Samples 2B and 4B increased in thickness, meaning that the SBF immersion induced the deposition of electrolyte species on the sample surface.

B. Morphology and chemical compositions

Figures 1 and 2 show the SEM micrographs of samples 2B and 4B before and after the Ht1 and 2. Comparing samples 2B and 4B, one can see that sample both samples present a relatively similar morphology. The porosity decreased after the Ht in both cases, suggesting the nucleation or precipitation of species due to the PEO coating/Ht solution interaction. The EDS results reveal that the coating compositions of all PEO coated samples have between 50 and 62%, in weight, of oxygen, 15 and 23% of

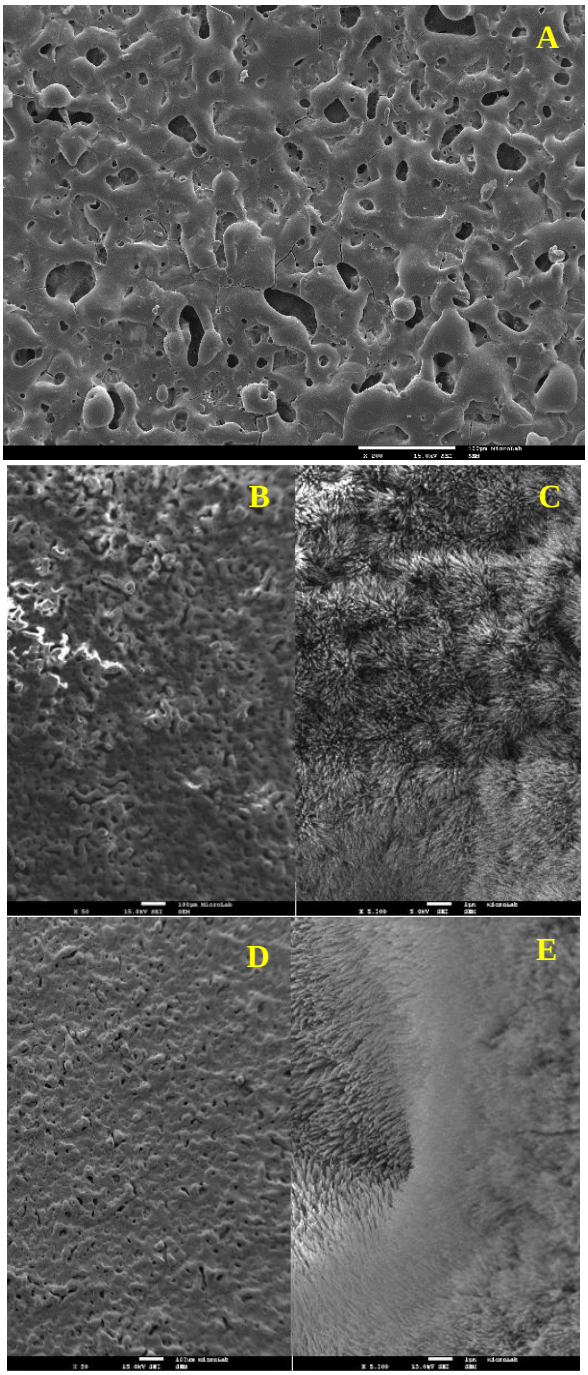

Figure 1 -SEM Micrographs of samples 2B (A – 200X), 2BHt$_1$ (B – 50X, C – 5000X), 2BHt$_2$ (D – 50X, E – 5000X).

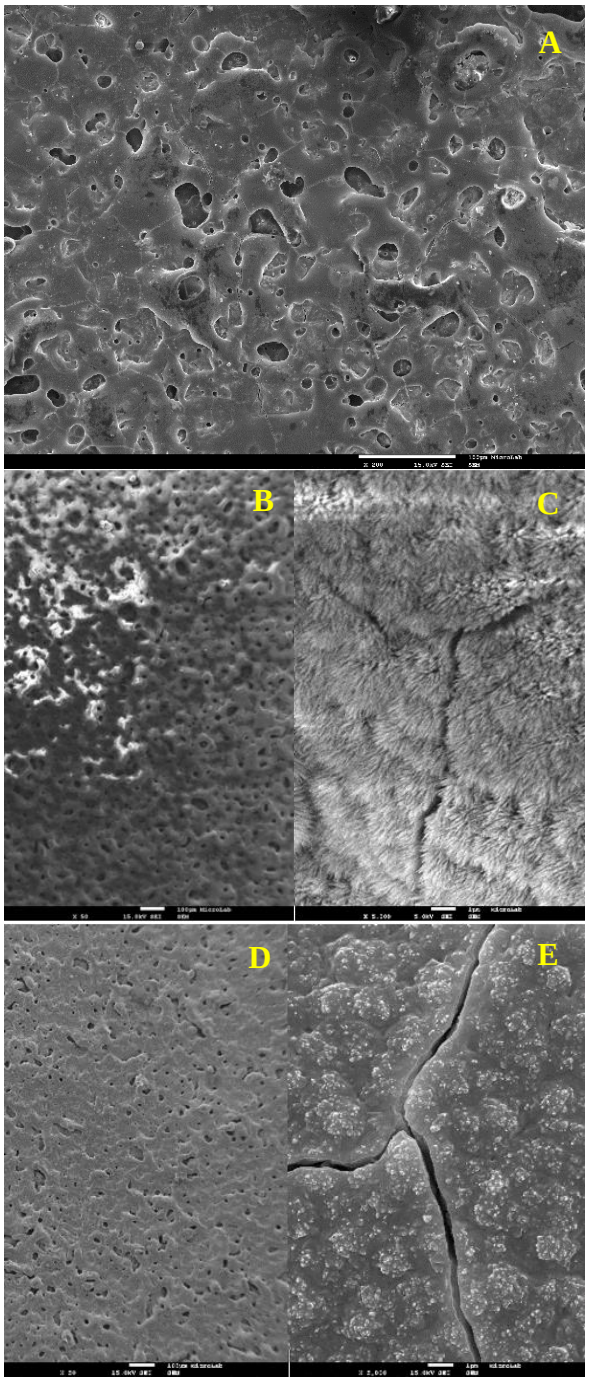

Figure 2 - SEM Micrographs of samples 4B (A – 200X), 4BHt$_1$ (B – 50X, C – 5000X), 4BHt$_2$ (D – 50X, E – 5000X).

magnesium, and between 8 and 20% of phosphorous. The amounts of calcium were about 5% on the samples coated with the calcium containing electrolyte, and between1 and 10% on the potassium containing electrolyte. The low amounts of calcium and phosphorous, high amounts of magnesium and oxygen suggest that the coatings are composed mainly of magnesium oxides/hydroxides, phosphates, and magnesium phosphates.

The EDS results of samples Ht samples, show that the coating is less than 1wt% magnesium, between 50 and 59wt% oxygen, low percentages of potassium and phosphorous and between 22 and 28wt% of calcium. Meaning that the ratio Ca/P close to 1.67 , which is the ratio of hydroxyapatite. The increase of thickness with both Ht´s and the chemical composition of the Ht coatings suggests the grow of hydroxyapatite [6]. Sample 4BHt$_2$, however, this needle like structures seen in all the other coatings, images 1C, 1E and 2C, does not appear in figure 2E,

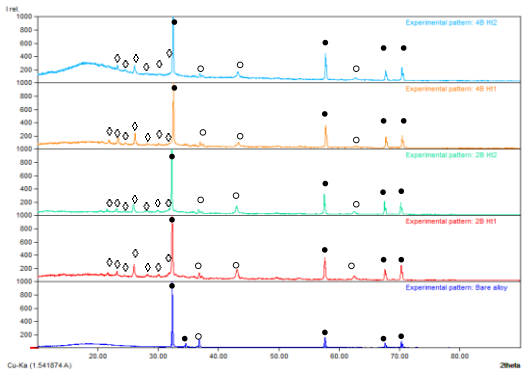

Figure 3 - XRD diffractograms of Ht samples before the immersion test; ◊ - HAp; ● – α-Mg; ○ – MgO; □ – Mg(OH)2.

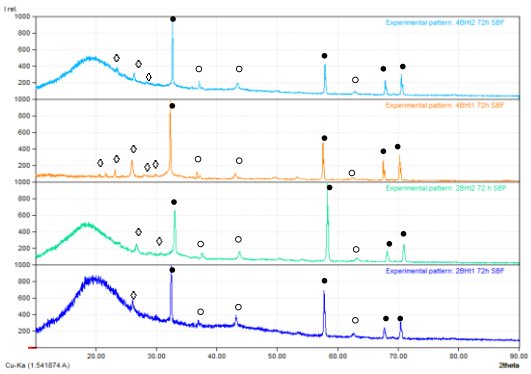

Figure 4 - XRD diffractograms of Ht samples after the immersion test; ◊ - HAp; ● – α-Mg; ○ – MgO; □ – Mg(OH)2.

suggesting, that in this case, more time is needed, or just a higher pH is needed for the hydroxyapatite nucleation.

Figure 3 shows the XRD results for the hydrothermally treated samples before the SBF immersion, and for comparison, the bare alloy XRD pattern was included in figure 3.

Because these coatings are only about 50µm thick, the XRD patterns show very intense peaks from the α-Mg phase.

Since the MAO coating is several tens of micrometres and the Ht coating is about five, a MgO phase also appeared in all the XRD patterns.

Several peaks of the Hap coating appear in the left side of the patterns, which is in accordance with the RDS results obtained for the same coatings. Sample $4BHt_2$ presented a more amorphous structure, as seen by the sample´s XRD pattern.

The XRD patterns obtained after the SBF immersion, in figure 4, apart from $4BHt_1$, all samples showed a more disorganized microstructure, even losing some of the peaks from the HAp coating, and, the increase in thicknesses in all samples after the SBF immersion suggest that there was some deposition SBF species on the Ht coatings.

The growth on both 2BHt coatings of needle like HAp suggests pH of the hydrothermal solution does not have a vital influence on the Hap nucleation and growing. However in the case of samples 4BHt, this cannot be said.

The EDS results for samples $2BHt_1$ and $2BHt_2$ after the SBF immersion showed a similar composition, which resulted in a Ca/P ratio of about 1.8. This suggests that there are some other calcium phosphates on the surface, but those are not seen in the XRD due to the noise. Figure 5 displays the micrographs of both 2BHt samples after the SBF immersion. A worm-like structure is seen in both, however, in the case of sample $2BHt_1$ the morphology is looser.

Sample $4BHt_1$ revealed a composition and ratio Ca/P similar to samples 2BHt, however, sample $4BHt_2$ revealed a needle like structure, in figure 6B, and a Ca/P ratio around 1.6, suggesting that in this case HAp structures have grown during the immersion time, and not in the hydrothermal treatment, like in sample $4BHt_1$. These results do not agree with the results of the XRD pattern, that show a more amorphous structure in sample $4BHt_2$, and sample $4BHt_1$ does no loose its crystallinity at all.

The disagreement between XRD patterns and SEM micrographs for samples after the SBF immersion can be a result of these HAp coatings being too thin compared to the PEO layer beneath them, which will also be too thin compared with the substrate, and hence being hard to read by the diffractometer.

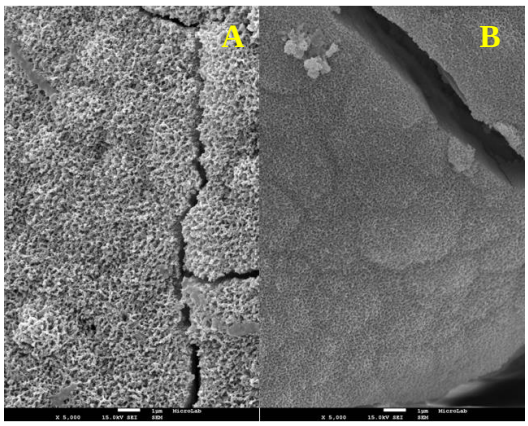

Figure 3 - 2BHt1 (A) and 2BHt2 (B) after 72 h of SBF immersion (5000X).

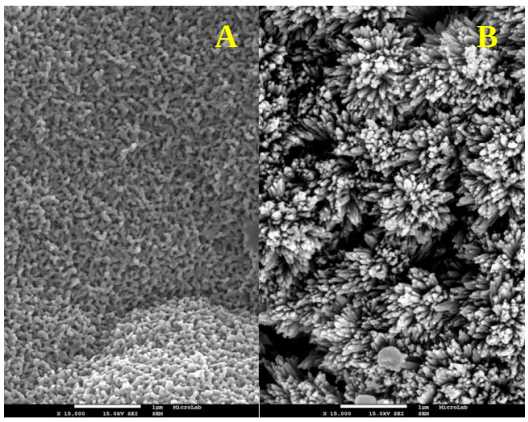

Figure 6 - $4BHt_1$ (A) and $4BHt_2$ (B) after 72 h of SBF immersion (15000X).

C. Corrosion behaviour

The Nyquist and Bode plots of all coated samples immersed in 0.1M NaCl is displayed in figure 7 and 8. The insert in figure 7 shows the impedance behaviour of the bare alloy, that shows a capacitive loop in the high/medium frequencies region and an inductive loop in the low frequencies. The capacitive loop is result of the double layer capacitance and the charge transfer resistance of the alloy, and the There is some controversy about the origin of the inductive behaviour present in the low frequencies region. Some authors say that it is due to the time needed for the relaxation of the adsorbed species on the substrate surface [7], whereas others propose that the inductive behaviour arises from the presence of intermediate species in the corrosion reaction of magnesium close to the substrate, meaning that before the formation of Mg^{2+}, the oxidation of Mg happens in several steps, and close to the surface, de-electronation of Mg^{+} into Mg^{2+}, for example, is not taken into account by the measurement equipment, and, because the presence of intermediate species can accelerate the overall reaction, the impedance values can decrease to negative values, and since this events require time to occur, those events would only have influence in the low frequencies region [8, 9].

All the coated samples behaved in a similar way, displaying two capacitance loops, one at high frequencies and one at low, exhibiting two time constants. The capacitance loops are attributed to the capacitance of the PEO coating, and the one in the low frequencies region is attributed to the double layer capacitance in the alloy/electrolyte interface. In the case of the coated samples, the inductive loop present in the bare alloy is not present, suggesting that the interaction between the alloy and the solution decreased substantially. The samples that showed a higher impedance response were samples 2B and 4B, hence those were chosen for the subsequent Ht and SBF immersion.

The phase angle plots in figure 8 confirms the two time constants and the magnitude plot display two capacitive behaviour both in high (assigned to the slope of approximately -1, which suggests an imperfect capacitor behaviour) and one at low frequencies, linked to the corrosion processes happening in the bottom of the pores [10].

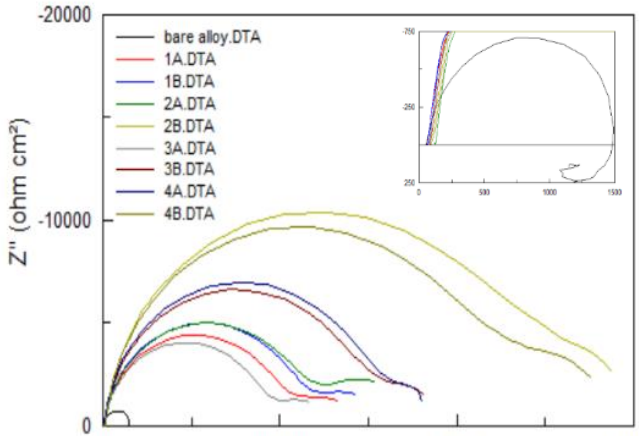

Figure 7 - Nyquist plots of bare alloy and coated samples immersed in 0.1M NaCl for 24h.

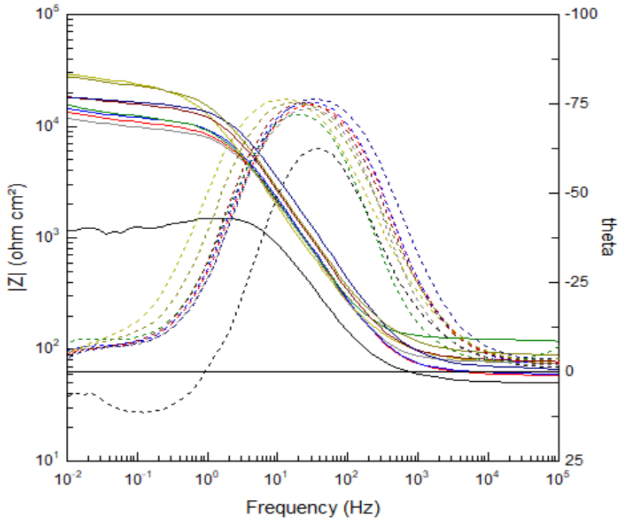

Figure 8 - Bode plots of bare alloy and coated samples immersed in 0.1M NaCl for 24h.

Two different equivalent circuits were proposed for the bare alloy and the coated samples. In order to model the pseudo-inductive behaviour shown by the bare alloy, a resistor (electrolyte resistance - Rs) in series with a constant phase element (CPEdl), which is an imperfect capacitor that takes into account the inhomogeneities of the samples surface and represents the double layer capacitance, the CPEdl is in parallel with another resistor (Rct), representing the charge transfer resistance. To model the pseudo inductive behaviour, in this work is proposed a negative resistor (Rads) and a negative capacitor (Cads), linked to the decrease in Rct double layer capacitance due to the adsorbed species during intermediary reactions. Figure 9 shows the equivalent circuit proposed.

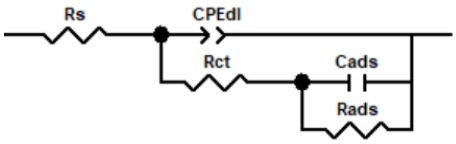

Figure 9 – Equivalent circuit proposed for the bare sample.

For the coated samples, since there is no inductive behaviour, the negative Cads and Rads were not added. The circuit proposed consists, as in figure 10, in adding a porous layer, modelled by a resistor, that represents the resistance of the electrolyte inside the PEO coating pores (Rp), in parallel with a CPEc, representing the capacitance of the PEO coating.

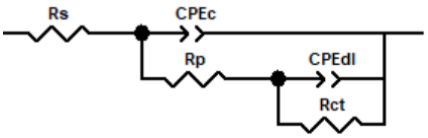

Figure 10 – Equivalent circuit proposed for the PEO coated samples in NaCl electrolyte.

The OCP curves of samples 2B and 4B immersed in SBF revealed that during the first five minutes, there is an accentuated decrease in potential of both samples, associated with the penetration of electrolyte in the coating pores. After that, there is a rapid shift in the noble direction which implies that the electrolyte starts to interact with the denser layer of the MAO coating.

After approximately one hour, both samples present a relatively stable potential, which indicates that the electrochemical reactions occurring between the solution and the coating are happening with a slow rate, suggesting that the coating pores were partially sealed by the corrosion products, and therefore a stable and saturated state.[11]

The OCP curves of both samples at 12, 24, 48 and 72 hours of immersion display a almost steady state behaviour, with small shifts in potential in the negative direction, for the first two daus, and then in the noble direction, between the second and the third day.

SBF is solution with a larger content in chlorides than the previous electrolyte, hence the Nyquist plots in figures 12 and 13 display a pseudo inductive behaviour. The equivalent circuit is shown in figure 11, in which the same negative RC used to model the inductive loop is added to the previous circuit.

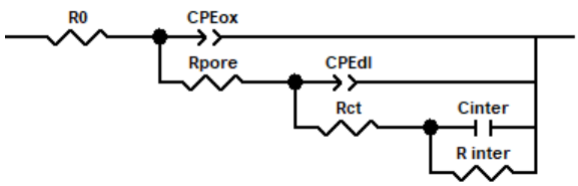

Figure 11 - Equivalent circuit proposed for the PEO coated samples in SBF.

The Nyquist plots shown in figures 12 and 14 show an accentuated decrease in impedance between the first 12h and the end of the first day, after that the decrease is less accentuated, and in the case of sample 4B there is an increase in the last 24 hours, suggesting the appearance of a protective film, or the formation of a stable MgO phase on the pores bottom.

Both plots show two capacitive loops in the high and medium frequencies, one in the low and an inductive one also in the low frequencies region. The capacitive loops are the result the capacitance of the MAO coating, and the substrate double layer capacitance. In both samples, the 72h impedance spectra and phase angle plot in figures 13 and 15 suggest the appearance of a fourth time constant in the high frequencies region, result of a competition between the dissolution and formation of compounds on the coatings surface, which is more accentuated on sample 2B than sample 4B. However, the introduction of another CPE on the equivalent circuit would give rise to a very

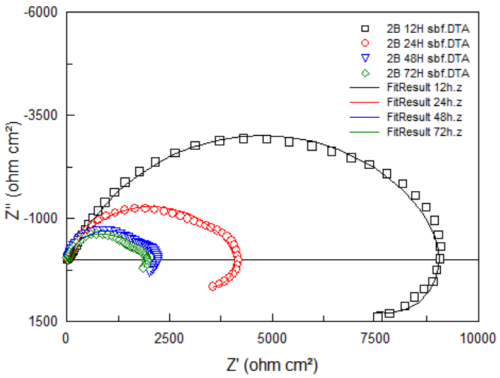

Figure 12 - 2B Nyquist plots for impedance in SBF.

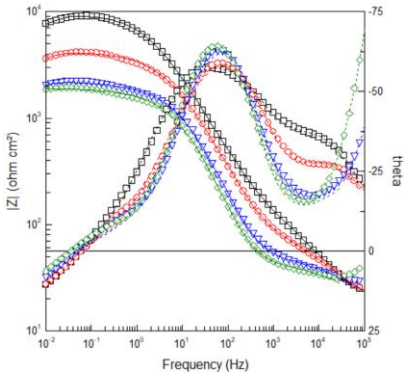

Figure 13 - 2B Bode plots for impedance in SBF

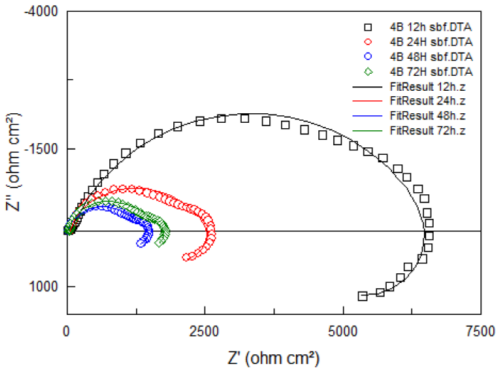

Figure 14 – 4B Nyquist plots for impedance in SBF.

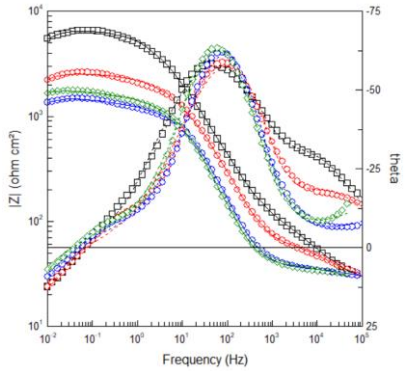

Figure 15 – 4B Bode plots for impedance in SBF.

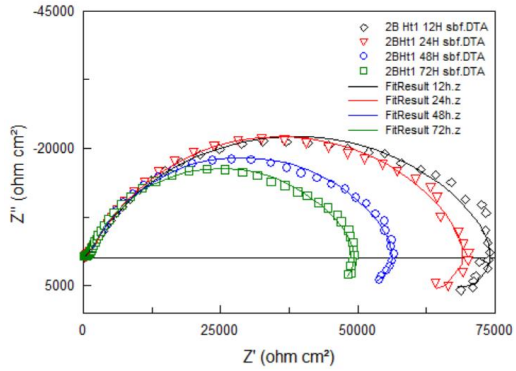

Figure 16 – 2BHt$_1$ Nyquist plots for impedance in SBF.

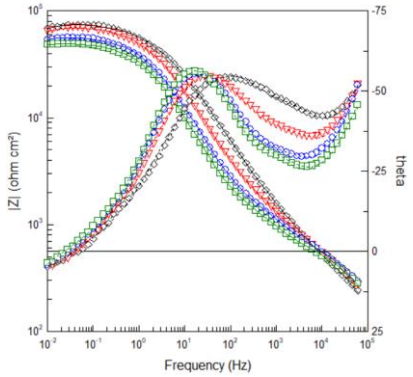

Figure 17 - 2BHt$_1$ Bode plots for impedance in SBF.

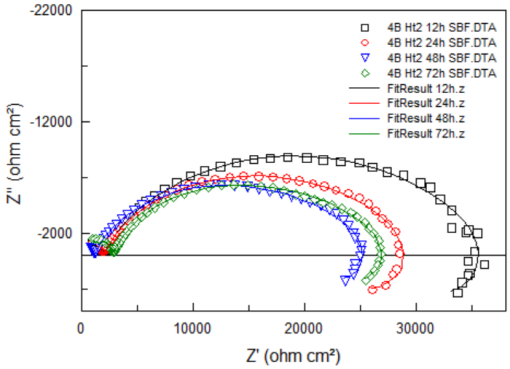

Figure 18 - 4BHt$_2$ Nyquist plots for impedance in SBF.

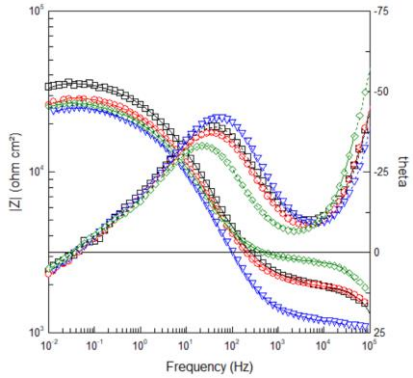

Figure 19 - 4BHt$_2$ Bode plots for impedance in SBF.

large fitting error, resulting in very large errors in the fitting parameters.

The immersion in SBF, in all samples, didn´t induce significant changes on the coating (macroscopically), however, in all samples except for 2BHt$_1$ and 4BHt$_2$, a localized attack occurred on the their surfaces, probably inside a larger pore on the previous MAO coating, or due to the adsorption of an insolubilized particle of the PEO electrolyte on the substrate surface, keeping the PEO coating from being formed on that spot. Resulting in the samples being corroded during the hydrothermal treatment. The corrosion that happen during the treatment removed the material required for the coating support on the surface thus enlarging the hole seen on the coating. The appearance of those holes suggests a probabilistic character on the efficiency of both the plasma anodization and the following hydrothermal treatment, and in this paper only the impedance data for the two samples that didn't suffered this localized attack is shown.

OCP curve of sample 2BHt$_1$, during the first seven hours, showed a relatively instable behavior, this may be due to the porous and inhomogeneous nature of the coating, and a competition between the dissolution and formation of new protective layers such as hydroxyapatite. After seven hours, the

OCP becomes stable, with a small slope towards the noble direction, indicating the existence on a steady state between the electrolyte and the coating. Sample 4BHt$_2$, on the other hand, started with a potential drop, during the first hour, probably due to the dissolution and rearrangement of protective layers, but after the first hour, the potential starts being shifted towards less negative values, indicating also, the growing or thickening of the present coating and the reaching of a steady state.

After the first 12h, the OCP of sample 2BHt$_1$ remains almost the same until the end of the second day. By the end of the third day there is a shift in potential in the noble direction, also indicating that the coating is improving its protection over time. In the case of sample 4BHt2, however, the OCP remains has a small decrease between the first and second day, and remains almost unchanged for the last two days, indicating also the existence of an equilibrium between the dissolution and formation of new films.

Since the hydrothermal treatment performed on samples 2B and 4B adds another layer on the protective coatings, the EIS results also display one more time constant, the Nyquist plots in figures 16 and 18 display three capacitive loops and one inductive. The first capacitive loop appears in the high frequencies region, probably due to the first layer of the coating, between the porous MAO and the electrolyte, the second capacitive loop appears also in the high frequencies region, and it is related with the MAO coating, beneath the hydroxyapatite layer. The third one results from the inner denser layer typical from anodization treatments, and the inductive loop, as

explained before, results from the adsorption of intermediate species in the corrosion reactions. Sample $2BHt_1$ displays a larger capacitance and resistance, as expected since in the OCP curves exhibit a more noble behavior. Despite of the suggestion of interaction between the substrate and the electrolyte given by the inductive loop, the impedance behavior does not change shape in the three days of immersion. Meaning that the coating is relatively resistant in a physiological environment. Sample $4BHt_2$ also presents the same behavior that sample $2BHt_1$, however, the Nyquist spectra of sample $4BHt_2$ show a bit higher impedance at 72 hours than at 48, implying that in this environment, the coatings pores are being sealed through the growing of a new layer of calcium phosphates.

The phase angle plots in figures 17 and 19 present a similar behavior in both samples. The phase angle diagrams present four time constants, two in the high frequencies region, one in the middle and one in the low. The Bode plots in figures 17 and 19, however, display a slightly different response, in sample $2BHt_1$, the impedance modulus increases in a faster rate since the higher frequency point, and the $4BHt_2$ presents a plateau between the 10^5 and 10^3 Hz, meaning that in the first case the substrate is protected from the electrolyte, and the coatings capacitance dominates the overall impedance values. In the case of sample $4BHt_2$, the plateau in the high frequencies region suggests the existence of a larger contribution of electrolyte and charge transfer resistances, meaning a less efficient protection [12].

On the other hand, the impedance measured at 72 hours of immersion on sample $4BHt_2$ displays an evolution towards a behavior similar to sample $2BHt_1$. Meaning that despite of being less efficient in protection of the alloy during the first stages of immersion, $4BHt_2$ coating exhibits a faster rate in growing a protection layer.

The equivalent circuit proposed for these samples is shown in figure 20. In this circuit, CPEHp represents the coating's top layer, created by the hydrothermal treatment. The Rphp represents solution resistance inside the pores within this layer. The rest of the circuit is similar to the one proposed for the PEO coatings fitting in SBF.

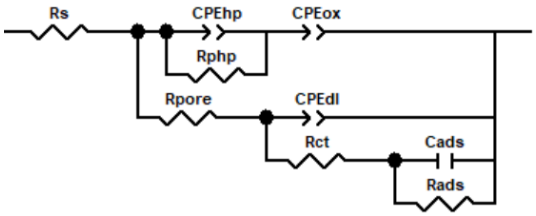

Figure 20 - Equivalent circuit proposed for fitting impedance data of samples 2BHt1 and 4BHt2.

The parameter of greater importance in all equivalent circuits is the charge transfer resistance, since the rate of all the corrosion reactions in the substrate/electrolyte interface is controlled by this parameter.

In the case of PEO samples immersed in NaCl solution, Rct increased one order of magnitude in all samples, compared to the bare alloy.

In the case of samples immersed in SBF, coparing sample Ht with PEo coated samples, there is also an increase on one order of magnitude, meaning that even less area is exposed to the electrolyte. Apart from sample $2BHt_1$, that showed an almost constant decrease with time, all samples displayed a charge transfer resistance almost constant, after the decrease I the first 24h. The increase in Rct of all treated samples, suggests that the corrosion protection provided by this samples is efficient.

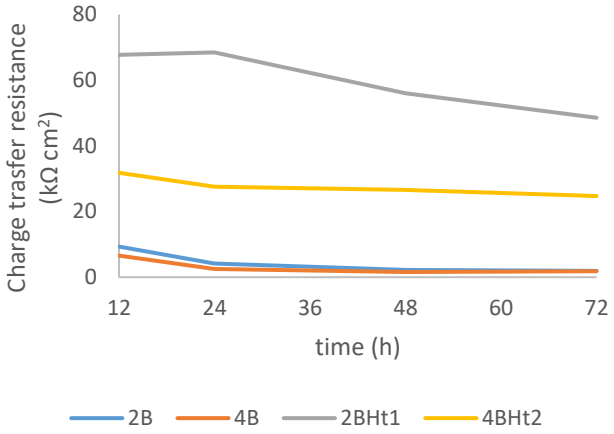

Figure 21 – Evolution of the Rct with immersion times in all samples immersed in SBF.

All micrographs and fitting results for the equivalent circuits of samples that are spoken but do not appear in this work are published elsewhere [13].

III. CONCLUSIONS

The results of the present work related with the PEO coatings are summarized here:

- Plasma electrolytic anodization produces a thick porous coating composed of oxides/hydroxides on the sample surface, and the thickness and porosity of such coating increases with the increase of both solution concentration and current intensity.
- EIS in 0.1 NaCl solution revealed that thicker coatings with denser barrier layers increase the alloy corrosion resistance for, at least, one order of magnitude by substantially diminishing the exposed area.
- The effectiveness of the PEO coatings protection was also confirmed by the absence of inductive behaviour in the NaCl solution EIS.
- Immersion in SBF decreases, slightly, the pores diameter by deposition of electrolyte species.
- OCP measurements in SBF revealed, at first, the deposition and formation of a protective film, and after, an equilibrium between dissolution and formation of such films. Resulting in an increasing corrosion resistance with time due to the slight decrease in the pores diameter.

- EIS in SBF showed an extra time constant in the low frequencies region, due to the aggressivity of the chlorides concentration in the solution and confirmed the OCP results that the samples corrosion resistance increases with time.
- PEO sample made with KOH (2B) showed a higher corrosion resistance in all impedances, however, the sample made with Ca(OH)2 (4B) displayed a higher increase in corrosion resistance.
- SBF immersion decreased the thickness of sample 2B and increased the thickness of sample 4B, suggesting that in spite of being more protective, sample 2B has less biocompatible than sample 4B.
- The efficiency of this coating is highly dependent of hydrodynamic conditions.

The results related with the hydrothermal treatment made on top of the selected PEO coated samples is listed below:

- The hydrothermal treatment after on top of the PEO coating slightly increases the thickness and decreases the pore diameter and density on the coating through the precipitation and nucleation of needle-like hydroxyapatite structures on the PEO surface.
- OCP measurement reveals a competition between dissolution and formation of a protective film, that after, it reaches an equilibrium.
- EIS revealed another time constant belonging to the hydroxyapatite layer on top of the PEO one, confirming the existence of a new protective layer.
- SBF immersion decreases the crystallinity degree of the coating, making it more similar to actual bone.
- EIS evolution with time suggests that in spite of being more corrosion resistant, sample 2BHT1 is less biocompatible than sample 4BHt2.

Related with this work, an evaluation of the corrosion behavior by another method, like potentiodinamic polarization, or hydrogen evolution is vital so the mass loss per time could be obtained, further research in cell attachment, osteoconductive and immersion in SBF for longer periods is needed.
The substantial improves of AZ31 alloy corrosion resistance, in physiological conditions, with out the use of any toxic element besides the aluminium present in the alloy proofs that the production of biodegradable bone implants is not far from reality.
Improvements to the results obtained here would be a coating produced in an electrolyte with substances more soluble, to decrease the hydrodynamic conditions influence on the overall results, an alloy with out any toxic substances, like Mg-Ca.

ACKNOWLEDGMENT (HEADING 5)

I would like to express my gratitude to Prof. João C.S. Fernandes for his supervision and scientific inputs, and Dr. Marta Alves, for her help in SEM – EDS characterization.

REFERENCES

[1] D. G. Poitout, *Biomechanics and Biomaterials in Orthopedics*. 2004.

[2] F. Haddad and a Cohen, *Joint Replacement*, no. July. 2009.

[3] E. García-Gareta, M. J. Coathup, and G. W. Blunn, "Osteoinduction of bone grafting materials for bone repair and regeneration," *Bone*, vol. 81, pp. 112–121, 2015.

[4] Z. Sheikh, S. Najeeb, Z. Khurshid, V. Verma, H. Rashid, and M. Glogauer, "Biodegradable materials for bone repair and tissue engineering applications," *Materials (Basel).*, vol. 8, no. 9, pp. 5744–5794, 2015.

[5] M. Saini, "Implant biomaterials: A comprehensive review," *World J. Clin. Cases*, vol. 3, no. 1, p. 52, 2015.

[6] S. V. Dorozhkin, "Calcium orthophosphate coatings on magnesium and its biodegradable alloys," *Acta Biomater.*, vol. 10, no. 7, pp. 2919–2934, 2014.

[7] G. Baril, G. Galicia, C. Deslouis, N. Pébère, B. Tribollet, and V. Vivier, "An Impedance Investigation of the Mechanism of Pure Magnesium Corrosion in Sodium Sulfate Solutions," *J. Electrochem. Soc.*, vol. 154, no. 2, p. C108, 2007.

[8] L. G. Bland, A. D. King, N. Birbilis, and J. R. Scully, "Assessing the corrosion of commercially pure magnesium and commercial AZ31B by electrochemical impedance, mass-loss, hydrogen collection, and inductively coupled plasma optical emission spectrometry solution analysis," *Corrosion*, vol. 71, no. 2, pp. 128–145, 2015.

[9] M. Curioni, F. Scenini, T. Monetta, and F. Bellucci, "Correlation between electrochemical impedance measurements and corrosion rate of magnesium investigated by real-time hydrogen measurement and optical imaging," *Electrochim. Acta*, vol. 166, pp. 372–384, 2015.

[10] P. Tian, X. Liu, and C. Ding, "In vitro degradation behavior and cytocompatibility of biodegradable AZ31 alloy with PEO/HT composite coating," *Colloids Surfaces B Biointerfaces*, vol. 128, pp. 44–54, 2015.

[11] H. Duan, K. Du, C. Yan, and F. Wang, "Electrochemical corrosion behavior of composite coatings of sealed MAO film on magnesium alloy AZ91D," *Electrochim. Acta*, vol. 51, no. 14, pp. 2898–2908, 2006.

[12] E. Barsoukov and J. R. Macdonald, *Impedance Spectroscopy*. 2005.

[13] F. P. S. Albuquerque, "Magnesium AZ31 alloy coating for bone implant applications," no. November, 2018.